Valence instability and crystal structures in $YbCu_xGa_{2-x}$ studied by x-ray absorption spectroscopy and x-ray diffraction

Hitoshi Yamaoka,[1,2,*] Yuichi Michiue,[3] Yoshiya Yamamoto,[4,†] Naohito Tsujii,[3,‡] Masashi Arita,[5] Hitoshi Sato,[5] Masahiro Sawada,[5] Hirofumi Ishii,[6] Nozomu Hiraoka,[6] and Jun'ichiro Mizuki[4,§]

[1]*RIKEN SPring-8 Center, 1-1-1 Kouto, Sayo, Hyogo 679-5148, Japan*

[2]*Institute for R&D Promotion, Doshisha University, Kyoto 602-8580, Japan*

[3]*International Center for Materials Nanoarchitectonics, National Institute for Materials Science, Sengen 1-2-1, Tsukuba 305-0047, Japan*

[4]*Graduate School of Science and Technology, Kwansei Gakuin University, Sanda, Hyogo 669-1337, Japan*

[5]*Hiroshima Synchrotron Radiation Center, Hiroshima University, Higashi-Hiroshima, Hiroshima 739-0046, Japan*

[6]*National Synchrotron Radiation Research Center, Hsinchu 30076, Taiwan*

(Received 2 July 2024; revised 28 September 2024; accepted 17 October 2024; published 13 November 2024)

The electronic and crystal structures of $YbCu_xGa_{2-x}$ under pressure were investigated by high-resolution x-ray absorption spectroscopy (XAS) at the Yb-L_3 absorption edge and x-ray diffraction. A rapid valence transition was found in $YbCu_{0.5}Ga_{1.5}$ around 5 GPa accompanying the structural phase transition. In YbCuGa and $YbCu_{1.5}Ga_{0.5}$ the Yb valence increased gradually up to 5–7 GPa and 16 GPa with pressure, respectively, and did not show a significant change above those pressures. XAS study at the Cu-L absorption edge was also performed. The major hybridization partner of Yb $4f$ electrons switched from Ga to Cu with increasing the Cu content around $x = 1$–1.5, where the c–f hybridization was weakest. Photoelectron spectroscopy was performed around Yb $4d$–$4f$ resonance energy and at 8.4 eV.

DOI: 10.1103/PhysRevB.110.205129

I. INTRODUCTION

Material properties strongly correlate to the degree of freedom of electrons such as spin, orbital, and charge. In intermetallic compounds, valence fluctuation provides an additional degree of freedom induced by temperature, chemical substitution, and pressure. The rare-earth intermetallic compounds of Ce, Sm, Eu, and Yb systems have often shown valence fluctuation, which depends on the hybridization between the localized $4f$ electrons and itinerant conduction electrons (c–f hybridization) and the hybridization strength is characterized by the Kondo temperature (T_K) [1]. The physical property of the compounds is described within a frame of Doniach phase diagram where the interplay between the Ruderman-Kittel-Kasuya-Yosida (RKKY) interaction and the Kondo effect has been observed [2–6]. In the vicinity at which both interactions compete is called a quantum critical point (QCP) where a magnetic phase transition is suppressed and anomalous and exotic physical properties such as unconventional superconductivity or non-Fermi liquid state have been observed.

Ce- and Yb-containing ternary intermetallics of *RE*-*M*-*X* (*RE* = Ce, Yb; *M* = transition metal; *X* = main group) often reveal the intermediated valence state. In Yb-containing ternary intermetallics, Yb-*M* gallides have been extensively studied for the past three decades, for example in Yb*T*Ga (*T* = Mg, Cu, Pd, Ag, Pt, Au) [7–12], $YbAgGa_2$ [11,13], $YbAu_xGa_{2-x}$ [14], $YbCu_{5-x}Ga_x$ [15], $YbCuGa_3$ [16], $YbNiGa_4$ [11,17], $YbNi_3Ga_9$ [18–22], $Yb_2Ru_3Ga_{10}$ [23], and $Yb_2Pt_6Ga_{15}$ [24]. Among them, the Yb-Cu-Ga and Yb-Ni-Ga systems have attracted much interest because of their interesting physical properties such as heavy fermion behavior, mixed valence, and quantum criticality induced by chemical substitution or pressure. While most papers have been focused on the synthesis of new samples and the study of the transport properties such as resistivity, specific heat, and magnetic susceptibility with x-ray diffraction (XRD) patterns to determine the crystal structures.

Pressure could control T_K and induce evolution from nonmagnetic fermi liquid to magnetic state through QCP. High-pressure studies have been performed for YbAuGa [11], $YbAgGa_2$ [11,13], $YbNi_3Ga_9$ [18–20], and $YbNiGa_4$ [11,17]. Electronic structures are also important clarifying the origin of the physical properties. However, studies of the electronic structures were limited to $Yb_2Pt_6Ga_{15}$ [24] at ambient pressure and $YbAgGa_2$ [13], $YbNiGa_4$ [11,17], $YbNi_3Ga_9$ [20,21], and $YbNi_3Ga_9$ [20] under pressure. Pressure dependence of the detailed electronic structure has not been explored even for the most simple Yb*T*Ga systems.

YbCuGa is known to also show valence fluctuation with an orthorhombic $CeCu_2$-type crystal structure [7,8]. Magnetic susceptibility showed a broad maximum of around 190 K

*Contact author: hitoshi_yamaoka@mineo.jp

†Present address: Nagoya Institute of Technology, Nagoya, Aichi 466-8555, Japan.

‡Contact author: TSUJII.Naohito@nims.go.jp

§Present address: Center for Research Initiative, Kwansei Gakuin University, Sanda, Hyogo 669-1337, Japan.

[8], corresponding to the Kondo energy of 205 K measured by the inelastic neutron scattering [9]. Thermoelectric power also showed a minimum of around the same temperature range [8]. The mean Yb valence was estimated to be 2.61 from the fit to the magnetic susceptibility with the interconfiguration fluctuation (ICF) model [8]. Electrical resistivity (ρ) of the Fermi liquid follows a relation $\rho = \rho_0 + AT^2$ at low temperatures, where ρ_0, A, and T are residual resistivity attributed to impurity scattering, coefficient attributed to electron–electron scattering, and temperature, respectively. In YbCuGa, T^2 dependence of the electrical resistivity was observed at 4.2–92 K and thus Fermi liquid ground state was suggested [8]. The coefficient A in the T^2 dependence was estimated to be 0.0025 μΩ cm/K^2 [9].

In the Yb system, the Kondo temperature decreases with pressure, and the Yb valence shifts to Yb^{3+}; this is physically an interesting range that the magnetic order through QCP begins to appear. But in YbCuGa no measurement of the electronic structure was reported even at ambient pressure. In YbCuGa, it is also not known which of Cu or Ga would be a main partner of the hybridization with Yb.

In this study, we prepared samples with different composition ratios of Cu and Ga, $YbCu_xGa_{2-x}$, and aimed to clarify the chemical composition and pressure dependencies of the electronic structures and the hybridization as well, and their crystal structures, systematically. We employed a high-resolution x-ray absorption spectroscopy with partial fluorescence mode (PFY-XAS) at the Yb-L_3 absorption edge [25–27]. We found a very rapid valence transition of the Yb valence in $YbCu_{0.5}Ga_{1.5}$ around 5 GPa and the successive transitions in YbCuGa and $YbCu_{1.5}Ga_{0.5}$. Crystal structures of $YbCu_xGa_{2-x}$ under pressure have not been explored. We performed XRD study under pressure to ascertain whether the valence transition was accompanied by a structural phase transition. The rapid valence transition in Yb of $YbCu_{0.5}Ga_{1.5}$ accompanied the structural phase transition. Photoelectron spectroscopy (PES) and XAS at the Cu-L absorption edge were performed at ambient pressure.

II. EXPERIMENTS

Polycrystalline samples of $YbCu_xGa_{2-x}$ ($x = 0.5$, 0.8, 1.0, and 1.5) were prepared by melting in sealed niobium tubes and subsequent annealing. Stoichiometric amounts of pure elements of Yb (99.9%), Cu (99.99%), and Ga (99.99%) were sealed in Nb tubes by arc under an Ar atmosphere. The Nb tubes were sealed in evacuated quartz tubes, and were heated in an electric furnace at 1373 K for 3 hours and were further annealed at 973 K for 96 hours. These compounds have the orthorhombic KHg_2-type crystal structure with the space group of *Imma*. The Cu and Ga atoms are distributed on the 8c sites. Chemical compositions measured with electron probe micro-analyzer (EPMA) were $Yb_{32.9}Cu_{16.35}Ga_{50.75}$ for $x = 0.5$, $Yb_{32.7}Cu_{26.9}Ga_{40.4}$ for $x = 0.8$, $Yb_{32.8}Cu_{34.4}Ga_{32.8}$ for $x = 1.0$, and $Yb_{32.3}Cu_{51.6}Ga_{16.1}$ for $x = 1.5$. These are close to the intended chemical composition. When the chemical composition of Cu is fixed, the composition ratios of Yb and Ga, including errors, are $Yb_{0.92\pm0.04}Cu_{0.5}Ga_{1.50\pm0.04}$, $Yb_{0.92\pm0.14}Cu_{0.75}Ga_{1.24\pm0.09}$, $Yb_{0.90\pm0.13}Cu_{0.95}Ga_{1.04\pm0.27}$, and $Yb_{0.89\pm0.02}Cu_{1.5}Ga_{0.51\pm0.15}$. The errors in the Yb composition ratio are large, so it is not clear how much of the deficiency there actually is.

Pressure dependence of the x-ray diffraction patterns was measured at Taiwan beamline BL12B2, SPring-8, using a three-pin plate diamond anvil cell (DAC, Almax Industries) with a CCD detection system at room temperature. We took an arrangement of both incoming and outgoing x-ray beams passing through the diamonds with an incident photon energy of $h\nu = 18$ keV ($\lambda = 0.6888$ Å). A two-dimensional image of the CCD system was integrated by using the FIT2D program [28]. The diffraction patterns were analyzed by the JANA2006 program [29,30].

PFY-XAS measurements were performed at room temperature at the Taiwan beamline BL12XU, SPring-8. Details of the experimental setup have been published elsewhere [31,32]. The overall energy resolution was estimated to be about 1 eV around the emitted photon energy of 7400 eV from the elastic scattering. The high-pressure conditions were realized using a diamond anvil cell (DAC) with a Be-gasket and the pressure-transmitting medium was silicone oil. A membrane-controlled DAC was used for high-pressure experiments. The pressure was measured based on the Raman shift of the ruby fluorescence [33–35].

Soft x-ray PES was performed at the beamline BL-7, the Hiroshima Synchrotron Radiation Center (HiSOR), equipped with a hemispherical electron-energy analyzer (Gammadata-Scienta SES-2002). In the soft x-ray PES the energy resolution (ΔE) was set to 40–50 meV around $h\nu = 182$ eV under the vacuum pressure below 10^{-8} Pa. The Fermi edge of Au on the sample holder was used to calibrate the binding energy. Samples were fractured in vacuum just before the measurements. The energy resolution and the Fermi level were determined with a fit of the Fermi edge of Au using a convolution of Gaussian and Fermi-Dirac functions. XAS study at the Cu-L absorption edge was performed at BL-14, HiSOR with the total electron yield mode, where the samples were fractured under the vacuum [36]. The energy resolution around 930 eV was set to be approximately 0.15 eV. It is noted that we could discuss the relative shift of the energy an order of magnitude lower than the resolution.

III. RESULTS

A. X-ray diffraction

The electronic states change significantly depending on the composition and pressure as we will show below. Therefore, it is important to investigate how the changes in the crystal structures correlate to those in the electronic states.

Figure 1 shows XRD patterns as a function of pressure for $YbCu_{0.5}Ga_{1.5}$, YbCuGa, and $YbCu_{1.5}Ga_{0.5}$. $YbCu_{0.5}Ga_{1.5}$ shows a phase transition at the pressure between 5.5 and 7.1 GPa.

$RCu_{0.8}Ga_{1.2}$ and $RCu_{0.5}Ga_{1.5}$ (R = Tm, Lu, both sides in the periodic table) were reported to have the crystal structures of KHg_2 type (space group *Imma*) and $CaIn_2$ type (space group $P6_3/mmc$), respectively [37]. For the case of R = Yb, $YbCu_{0.8}Ga_{1.2}$ has been reported to be of the KHg_2 type, similar to the case of R = Tm and Lu. For $YbCu_{0.5}Ga_{1.5}$, there is no report, but the XRD pattern shows that the KHg_2 type is

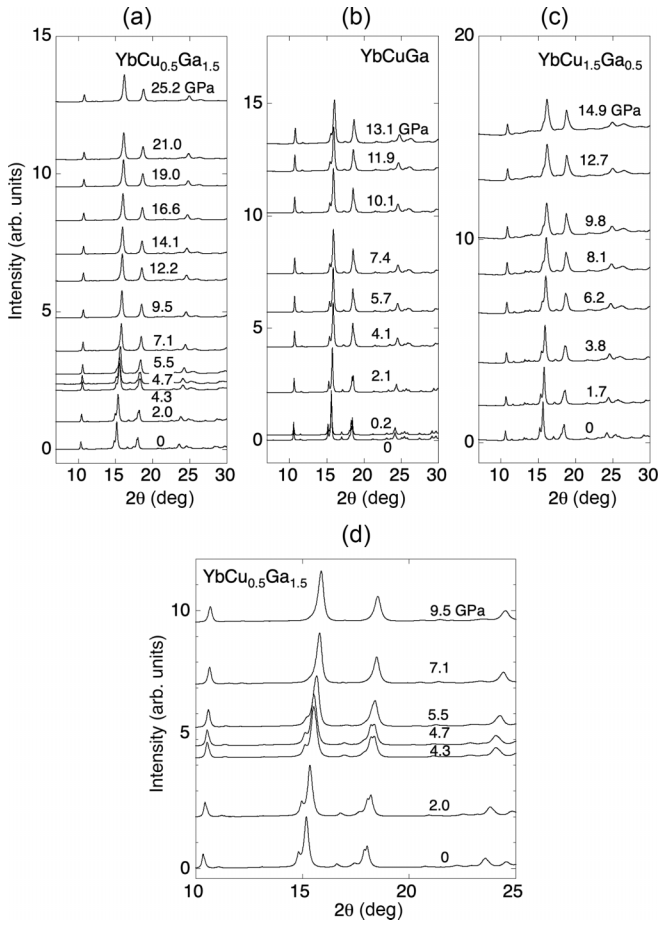

FIG. 1. . X-ray diffraction patterns of (a) $YbCu_{0.5}Ga_{1.5}$, (b) YbCuGa, and (c) $YbCu_{1.5}Ga_{0.5}$ at 300 K. The baseline height of each pattern scales to the measured pressure. In (d) we show an expanded view of the XRD patterns in (a) around the phase transition pressure of 5 GPa.

the most plausible. This is probably because of the large ionic radius of Yb caused by the valence fluctuation or the effect of the number of valence electrons in $YbCu_{0.5}Ga_{1.5}$. It may be reasonable that the crystal structure of $YbCu_{0.5}Ga_{1.5}$ undergoes a phase transition to the $CaIn_2$ type when approaching the Yb^{3+} state with pressure.

Diffraction data of YbCuGa and $YbCu_{1.5}Ga_{0.5}$ at all pressures were fitted by the structure model isotypic to $YbCu_{0.8}Ga_{1.2}$, which is the KHg_2-type structure of the space group *Imma* [37]. As for $YbCu_{0.5}Ga_{1.5}$, the KHg_2-type structure was taken at 4.74 GPa and below, while the diffraction patterns at 7.13 GPa and above were fitted by the model isotypic to $LuCu_{0.5}Ga_{1.5}$; namely, the $CaIn_2$-type structure of the space group $P6_3/mmc$ [37]. The pattern at 5.46 GPa resembles that at 7.13 GPa, but was insufficiently fitted by the $CaIn_2$-type model. Residual intensities were seen in the lower-angle region of the strong reflection peak at around 15.5°, which indicated the coexistence of the KHg_2-type structure. Thus, the diffraction pattern at 5.46 GPa was well fitted by assuming that the sample consists of two phases of $CaIn_2$ and KHg_2 types. Examples of the plots of the profile fitting are given in Fig. S1 within the Supplemental Material (SM)[38]. The results of structure refinements and final parameters are also summarized in Tables. S3–S6 within the SM [38].

Figures 2(a)–2(f) show the pressure dependence of the lattice constants and the volume. YbCuGa and $YbCu_{1.5}Ga_{0.5}$ kept the KHg_2-type structure up to approximately 13 and 15 GPa, respectively. While $YbCu_{0.5}Ga_{1.5}$ has a structural phase transition approximately at 5 GPa. Pressure-induced decrease of the lattice constants and the volume of $YbCu_{0.5}Ga_{1.5}$ is more rapid at the pressure less than 5 GPa compared to those of others and they become gradual after the structural transition as shown in Fig. 2(d). In Fig. 2(g) we summarize the pressure dependence of the type of the crystal structure in $YbCu_xGa_{2-x}$ including $YbGa_2$ [39]. $YbGa_2$ has the $CaIn_2$-type crystal structure at ambient pressure, while $YbCu_xGa_{2-x}$ has the KHg-type crystal structure with the space group of *Imma* at $x \geqslant 0.5$ ($x = 0.5$, 1.0, 1.5, and 2.0). Pressure dependence of the crystal structure for $YbCu_2$ was recently measured [40].

In Figs. 2(d)–2(f) we show fits of the pressure-volume relation by using the empirical formula of the Murnaghans equation of state widely used in the high-pressure research [41], $\frac{V}{V_0} = [1 + p\frac{B_0'}{B_0}]^{-\frac{1}{B_0'}}$, where V, V_0, B_0, and B_0' are volume, volume at ambient pressure, bulk modulus, and its first derivative with respect to the pressure, respectively. We obtain the parameters of $B_0 = 43.9$ GPa, $B_0' = 18.7$, $V_0 = 220.7$ Å^3 for $YbCu_{1.5}Ga_{0.5}$ and $B_0 = 66.4$ GPa, $B_0' = 22.1$, $V_0 = 221.6$ Å^3 for YbCuGa. In $YbCu_{0.5}Ga_{1.5}$ the parameters are estimated to be $B_0 = 54.8$ GPa, $B_0' = 6.84$, $V_0 = 240.0$ Å^3 at $p < 6$ GPa and $B_0 = 121$ GPa, $B_0' = 8.85$, $V_0 = 228.1$ Å^3 at $p > 5$ GPa.

B. Lattice constants and atomic distances

In Figs. 3(a)–3(c) we show x dependence of the lattice constants. x dependence of them is small at $x \geqslant 1.0$. Figures 3(d)–3(f) show x dependence of ratios of the lattice constants. Figure 3(g) shows the crystal structures of the KHg_2-type with the space group *Imma* and the $CaIn_2$-type with the space group $P6_3/mmc$. We estimated the atomic distances between Yb and M (Ga, Cu) at ambient pressure based on the results in Fig. 2. Crystallographically, there is only one site occupied by Cu and Ga in the model of space group *Imma*. We thus assumed that this site (M) is randomly occupied by Cu and Ga (at a ratio corresponding to the composition ratio of the sample). There are 12 relatively short-range M sites around one Yb. It means that M has 12 coordinates to Yb as shown in Fig. 3(g). These 12 interatomic distances (Yb–M) are classified into four types from $d1$ to $d4$, and there are two each for $d1$ and $d3$, and four for $d2$ and $d4$, 12 distances in total. They are the averaged distances of Yb–Cu and Yb–Ga. Therefore, in this case, the Yb–Cu and Yb–Ga distances in the crystal cannot be determined separately from the XRD analysis. Figure 3(h) is a plot of the above four types of Yb–M distances against the parameter x. The CIFs (crystallographic information files) of $YbCu_2$ and $YbCu_{0.8}Ga_{1.2}$ were found in ICSD (the Inorganic Crystal Structure Database) [42] and the interatomic distances calculated from them were also added. There is a trend that the distances decrease with increasing x. However, in $d1$ at $x = 0.8$ and $d2$ and $d3$ at $x = 1.5$, the Yb-M distance increases irregularly. Furthermore, the decrease

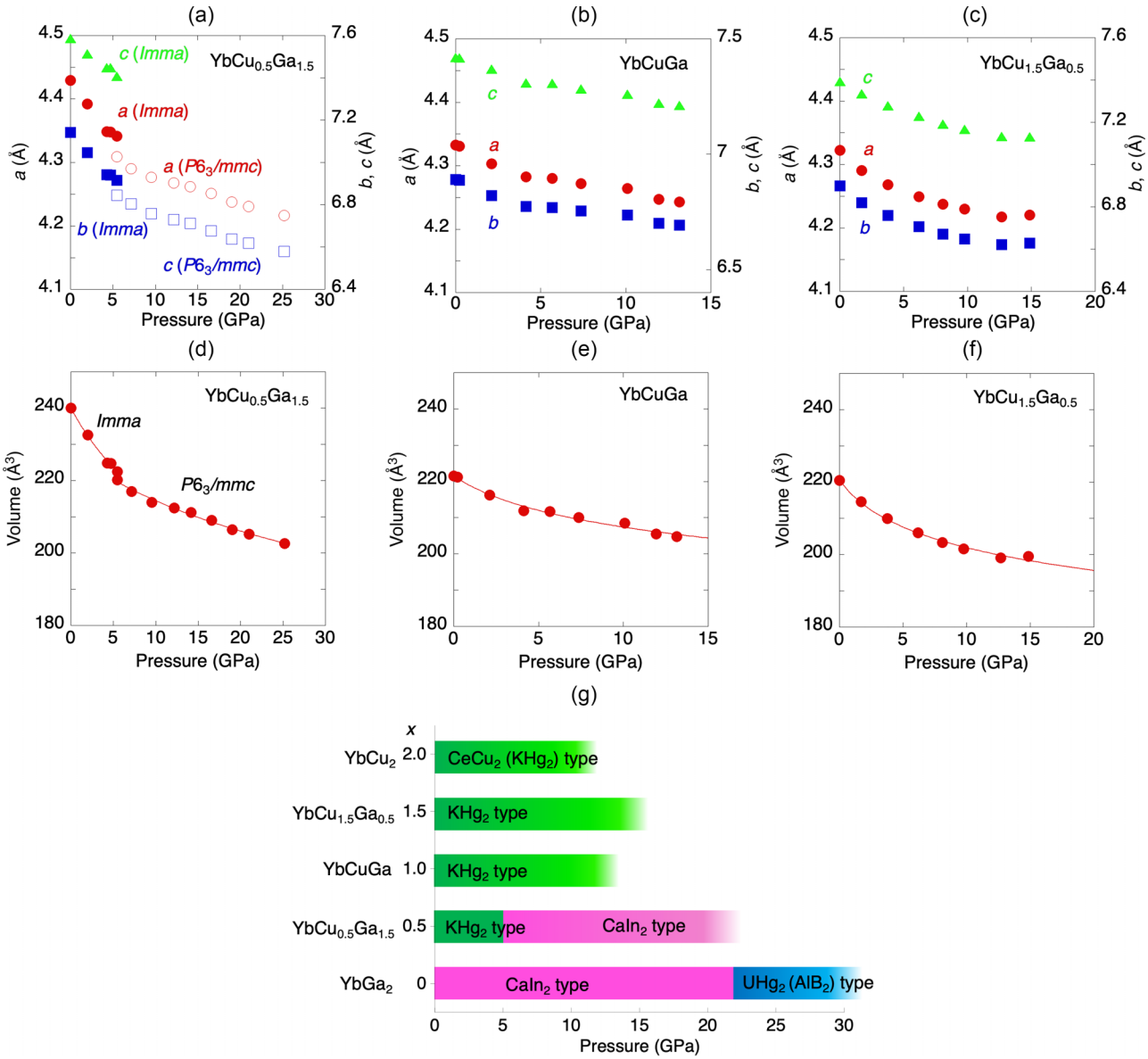

FIG. 2. (a)–(c) Pressure dependence of the lattice constants of (a) $YbCu_{0.5}Ga_{1.5}$, (b) YbCuGa, and (c) $YbCu_{1.5}Ga_{0.5}$. (d)–(f) Pressure dependence of the volume of (d) $YbCu_{0.5}Ga_{1.5}$, (e) YbCuGa, and (f) $YbCu_{1.5}Ga_{0.5}$. Solid lines are the fits by using the empirical formula of the Murnaghans equation of state [41]. (g) A summary of the pressure dependence of the type of the crystal structure in $YbCu_xGa_{2-x}$. $YbGa_2$ has a structural phase transition at 22 GPa [39]. The maximum pressures measured here were approximately 25, 13, and 15 GPa for $YbCu_{0.5}Ga_{1.5}$, YbCuGa, and $YbCu_{1.5}Ga_{0.5}$, respectively. In (a)–(f) the errors are within the size of the symbols.

of the atomic distances in $d1$ and $d4$ seems to slow down between $x = 1.5$ and 2. Here, the data at $x = 0.8$ estimated based on the table [37] seem not to be closely connected to the present measured results and thus, we do not discuss the anomaly of the Yb–M distances at $x = 0.8$. In Fig. 3(i) we show the atomic distances between Yb atoms against x. The Yb-Yb distance decreases monotonically with x.

Figure 3(j) shows the pressure dependence of the Yb–M distances in $YbCu_{0.5}Ga_{1.5}$. In the high-pressure phase of the $P6_3/mmc$ type, $YbCu_{0.5}Ga_{1.5}$ has one independent Yb site crystallographically. There are 12 M (= Cu or Ga) sites in the vicinity of Yb, and the distance between Yb and M is divided into two types ($d'1$ and $d'2$) each containing six atoms. In the $P6_3/mmc$ crystal structure, the change in the interatomic distance is relatively gradual and well corresponds to the contraction of the unit cell in Fig. 2(g) and gradual change in the Yb valence after the valence transition in Fig. 4(f) below. We observed the anomaly of the Yb–Cu distances just below the pressure range of the phase transition. Figure 3(k) shows the pressure dependence of the Yb–Yb distances in $YbCu_{0.5}Ga_{1.5}$. The Yb–Yb distances show smooth changes before and after the phase transition, compared to the case of the Yb–Cu distance.

Figures 3(l) and 3(m) show the pressure dependencies of the distances between the Yb atoms in YbCuGa and $YbCu_{1.5}Ga_{0.5}$, respectively. The distances between Yb atoms decrease monotonically with pressure. But there is an exception in Fig. 3(j) that the $d2$ in $YbCu_{1.5}Ga_{0.5}$ increases above

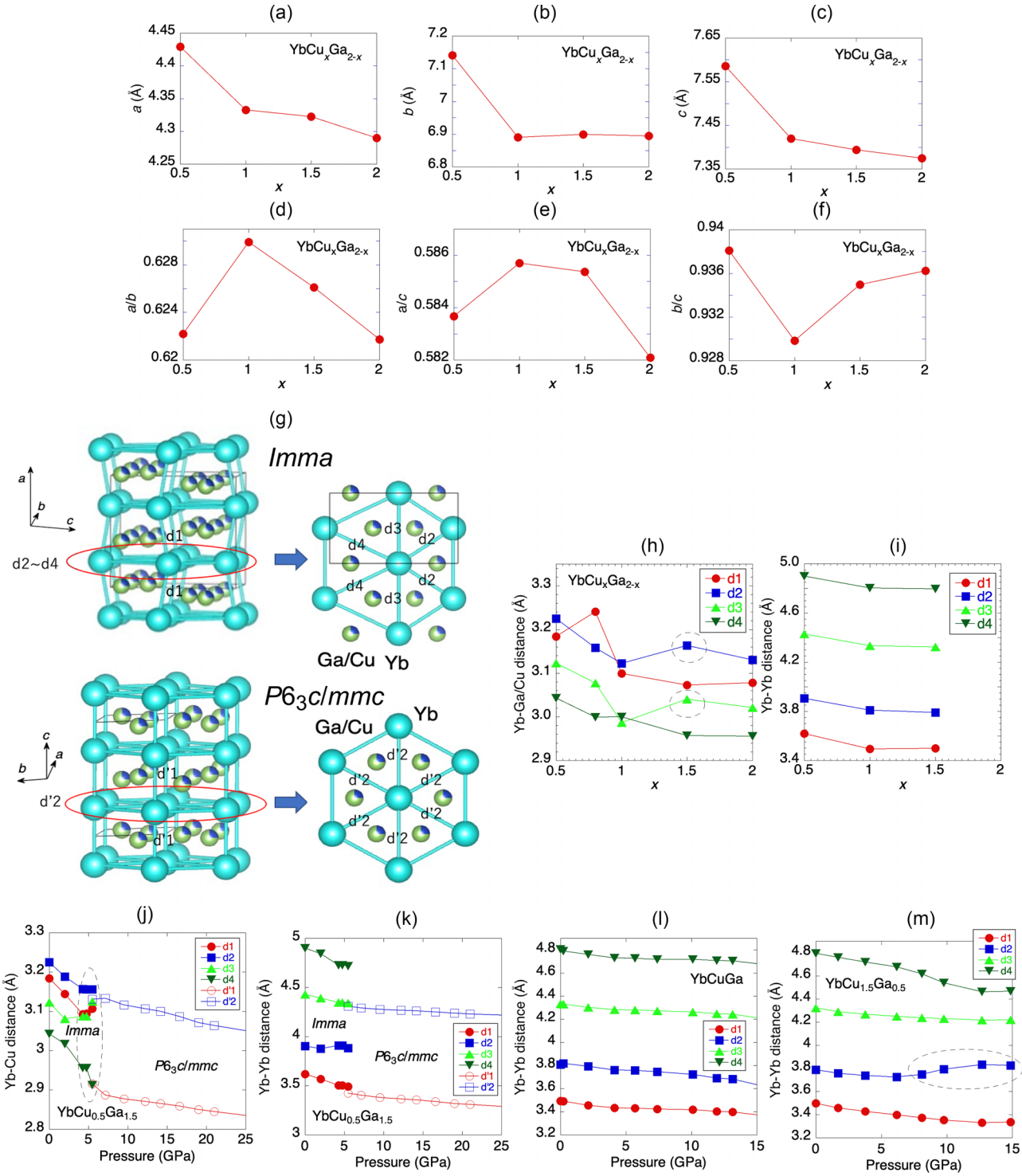

FIG. 3. (a)–(c) Chemical composition (x) dependence of the lattice constants at ambient pressure. (d)–(f) Ratio of the lattice constants, (d) a/b, (e) a/c, and (f) b/c. (g) Crystal structures and definition of the distances from $d1$ to $d4$ for the crystal structure of *Imma* type and $d'1$ and $d'2$ for that of $P6_3/mmc$ type, where d is the distance between Yb and M (Ga, Yb). (h)–(i) x dependence of the atomic distances of (h) Yb-Ga/Cu and (i) Yb-Yb estimated from the present XRD results. Note that the distances at $x = 0.8$ and 2.0 were estimated from the CIFs (Crystallographic Information Files) of $YbCu_2$ and $YbCu_{0.8}Ga_{1.2}$ in the Inorganic Crystal Structure Database [37]. In (h) dotted circles correspond to the data where pressure-induced anomalous changes occurred. (j)–(k) Pressure dependence of the atomic distances of (j) Yb-Cu and (k) Yb-Yb for $YbCu_{0.5}Ga_{1.5}$. (l)–(m) Pressure dependencies of the atomic distances of Yb-Yb are shown for (i) YbCuGa and (j) $YbCu_{1.5}Ga_{0.5}$. In (a)–(c) and (h)–(m) the errors are within the size of the symbols. In (j) and (m) dashed circles correspond to the data where anomalous changes were observed.

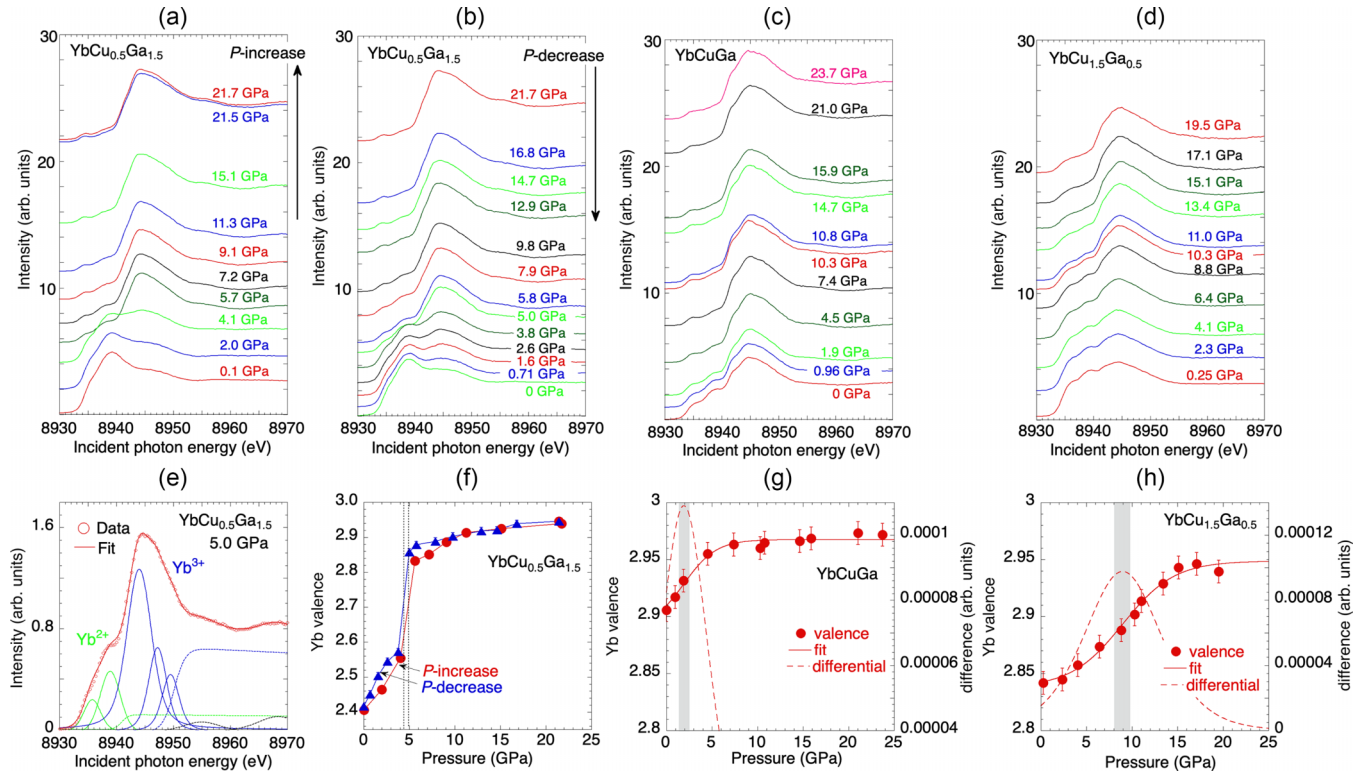

FIG. 4. (a)–(d) Pressure dependence of the PFY-XAS spectra of (a) $YbCu_{0.5}Ga_{1.5}$ with increasing the pressure, (b) $YbCu_{0.5}Ga_{1.5}$ with decreasing the pressure, (c) YbCuGa, and (d) $YbCu_{1.5}Ga_{0.5}$ at room temperature. The baseline height of each spectrum scales to the measured pressure. Panel (a) shows the spectra when the pressure was increased (*P*-increase), and panel (b) shows the spectrum when it was lowered (*P*-decrease). (e) An example of the fit to the PFY-XAS spectrum at 5.0 GPa of $YbCu_{0.5}Ga_{1.5}$. (f)–(h) Pressure dependence of the Yb valence of (f) $YbCu_{0.5}Ga_{1.5}$, (g) YbCuGa, and (h) $YbCu_{1.5}Ga_{0.5}$. The errors of the valences are of the order of ±0.01. In (f) closed circles and closed triangles correspond to the Yb valences when the pressure was increased (*P*-increase) and decreased (*P*-decrease), respectively. In (g) and (h) solid lines, dashed lines, and shaded areas are the fits to the Yb valence using the modified logistic curve, differential of the fitted curves, and critical pressure rages of the valence transition, respectively.

10 GPa as shown in Fig. 3(m) (dashed circles) although both the crystal structure and the Yb valence do not show any anomaly around 10 GPa.

C. Pressure dependence of Yb valence

Pressure dependence of the PFY-XAS spectra was measured at room temperature as a function of pressure for $YbCu_{0.5}Ga_{1.5}$, YbCuGa, and $YbCu_{1.5}Ga_{0.5}$ as shown in Figs. 4(a)–4(d). Figure 4(e) shows an example of the fits to the PFY-XAS spectrum of $YbCu_{0.5}Ga_{1.5}$ at 5.0 GPa. In the fits, we assumed some Voigt functions for each Yb component with the arctan-like backgrounds. The intensities of the two arctan-like backgrounds were determined to be proportional to the intensities of their corresponding Voigt functions of the Yb^{2+} and Yb^{3+} components. The mean valence is defined to be $v=2 + I(3+)/(I(2+) + I(3+))$, where $I(n+)$ is the intensity of Yb^{n+} component [43]. The errors of the valences are on the order of ±0.01.

Figure 4(f) shows the pressure dependence of the Yb valence for $YbCu_{0.5}Ga_{1.5}$. The Yb valence changes suddenly and significantly by about 0.3 around 5 GPa with a hysteresis. The hysteresis of the Yb valence, the change in the crystal structure, and the coexistence of two phases (i.e., the presence of latent heat) just near the critical pressure as shown in Fig. 2(d) may suggest a first-order valence transition. In practice, the volume fraction of the two phases of $YbCu_{0.5}Ga_{1.5}$ at 5.46 GPa was 36% for $CaIn_2$ type ($P6_3/mmc$) and 64% for KHg_2 type ($Imma$). However, the first-order valence transition should be confirmed through the measurements of the transport properties such as the resistivity.

In YbCuGa and $YbCu_{1.5}Ga_{0.5}$the Yb valence increased gradually up to 5–7 GPa and 16 GPa with pressure, respectively, and did not show a significant change above those pressures as shown in Figs. 4(g) and 4(h).

In Figs. 4(g) and 4(h) we approximate the pressure dependence of the Yb valence by a modified logistic curve which draws an S-shaped curve and the increase approaches nearly a constant value at high pressures [38]. The logistic curve has been used widely to represent many natural phenomena. Here, we define the pressure of the inflection point of the fit curves as the critical pressure of the valence crossover (P_v) for the pressure-induced successive valence transition. We also use P_v for the first-order valence transition.

In $YbCu_{0.5}Ga_{1.5}$ we observed a rapid increase of the Yb valence up to 5 GPa with pressure and after the valence transition, the Yb valence does not change much. We also measured the PFY-XAS spectra by decreasing the pressure as shown in Fig. 4(b). The results show a hysteresis of the pressure-induced change in the Yb valence in Fig. 4(f), indicating

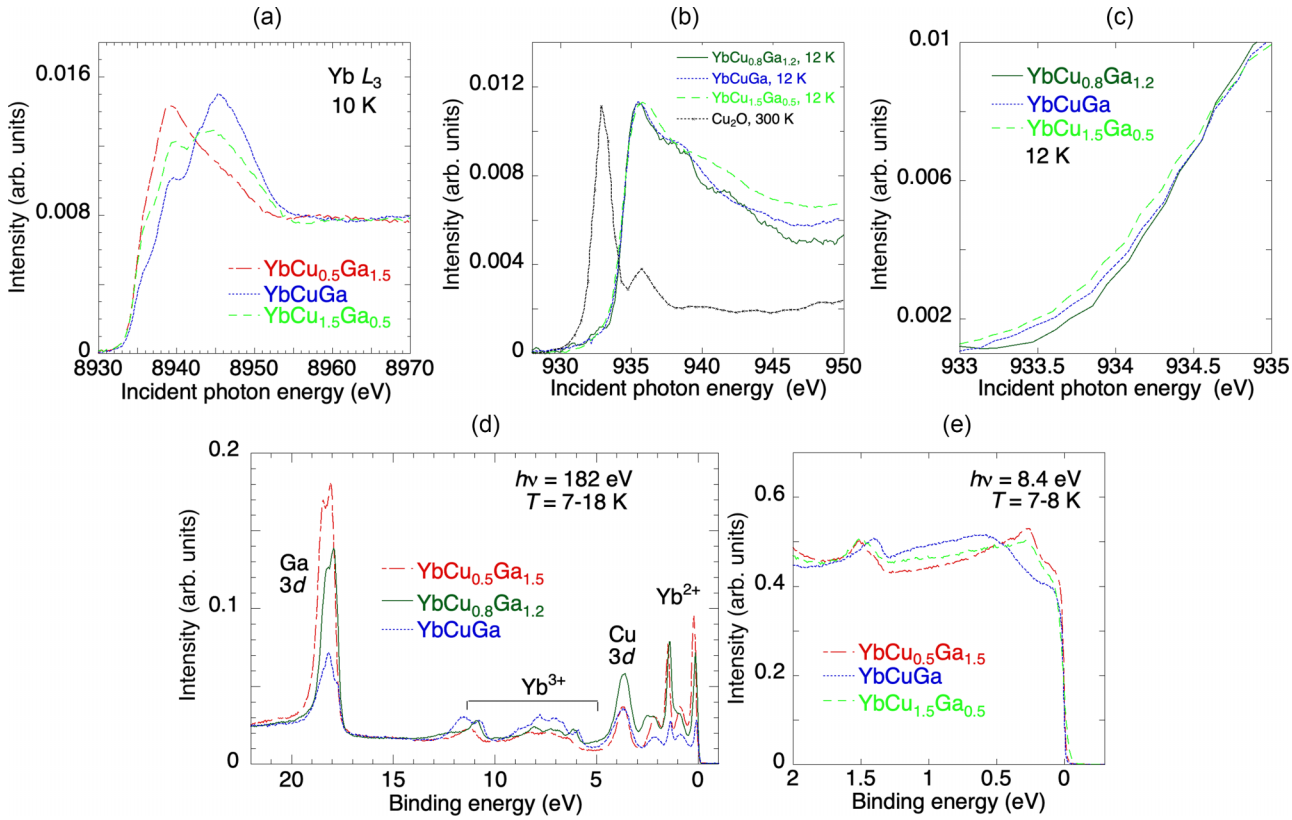

FIG. 5. (a) PFY-XAS spectra of $YbCu_{1.5}Ga_{0.5}$, YbCuGa, and $YbCu_{0.5}Ga_{1.5}$ at 10 K and at the Yb-L_3 absorption edge. (b) X-ray absorption spectra of $YbCu_{0.8}Ga_{1.2}$, YbCuGa, and $YbCu_{1.5}Ga_{0.5}$ at the Cu K absorption edge and 12 K with that of Cu_2O at 300 K for comparison. (c) Enlarged figure of (b) near the absorption edge. (d) Valence band spectra of $YbCu_{0.5}Ga_{1.5}$, $YbCu_{0.8}Ga_{1.2}$, and YbCuGa at $h\nu = 182$ eV and 7–18 K. (e) Valence band spectra of $YbCu_{0.5}Ga_{1.5}$, YbCuGa, and $YbCu_{1.5}Ga_{0.5}$ near the Fermi level at the incident photon energy $h\nu = 8.4$ eV (Xe lamp) and 7–8 K.

the first-order valence transition. The valence transition pressure coincides with the structural phase transition observed in the XRD measurements. Therefore, this valence transition originates from the structural phase transition. Meanwhile, in the other two compounds of YbCuGa and $YbCu_{1.5}Ga_{0.5}$ no structural phase transition was observed as described above. Mean Yb valences at the ambient pressure were estimated to be 2.46 for $YbCu_{0.5}Ga_{1.5}$, 2.91 for YbCuGa, and 2.84 for $YbCu_{1.5}Ga_{0.5}$, where the errors are on the order of ± 0.01. This value for YbCuGa is in contrast to the value of 2.61 estimated from the fit to the magnetic susceptibility with the ICF model by Adroja *et al.* [8]. The ICF model assumed the thermal population of two different valence states. However, the inelastic neutron scattering showed the Kondo energy of 205 K [9], suggesting the dominant role of the Kondo interaction on the Yb valence state through the hybridization between f and conduction electrons. Therefore, the value of the Yb valence based on the ICF model may be underestimated.

In $YbCu_xGa_{2-x}$ the lattice constants and the unit cell volume increase with decreasing the Cu content x at ambient pressure. On the other hand, the critical transition pressure seems not to correlate to the change in the lattice constants and the volume. Furthermore, the Yb valence increases with increasing x up to $x = 1.0$, does not show a remarkable change between $x = 1.0$ and 1.5, but decreases rapidly between $x = 1.5$ and 2.0 at ambient pressure. We discuss the chemical composition dependence of the Yb valence in detail in the Discussion below.

D. XAS spectra at the Cu-L absorption edge and the valence band spectra

It is also important to know the electronic states of Ga/Cu because it gives complementary information to the electronic states of the Yb sites. We measured the XAS spectra at the Yb-L_3 absorption edge with those at the Cu-L absorption edge at low temperatures. Photoelectron spectroscopy was also performed at low temperatures.

Figure 5(a) shows the comparison of the PFY-XAS spectra for $YbCu_{0.5}Ga_{1.5}$, YbCuGa, and $YbCu_{1.5}Ga_{0.5}$ at 10 K at the Yb-L_3 absorption edge. The intensity is normalized by the area. In $YbCu_{0.5}Ga_{1.5}$ divalent Yb component is dominant, while in $YbCu_{1.5}Ga_{0.5}$ and YbCuGa the intensity of the trivalent Yb component becomes stronger.

We also measured the XAS spectra of Cu at the Cu-L absorption edge and at 12 K with the total fluorescence yield mode for $YbCu_{1.5}Ga_{0.5}$, YbCuGa, and $YbCu_{0.8}Ga_{1.2}$ as shown in Fig. 5(b). The intensity is normalized to the peak. In Fig. 5(b) we also show the spectra of Cu_2O ($3d^{10}$) at 300 K as a reference. The spectrum of Cu_2O reproduced well the previous results [44]. The absorption edges of $YbCu_xGa_{2-x}$ shift to higher energies than those of CuO ($3d^9$) and Cu_2O [44–46],

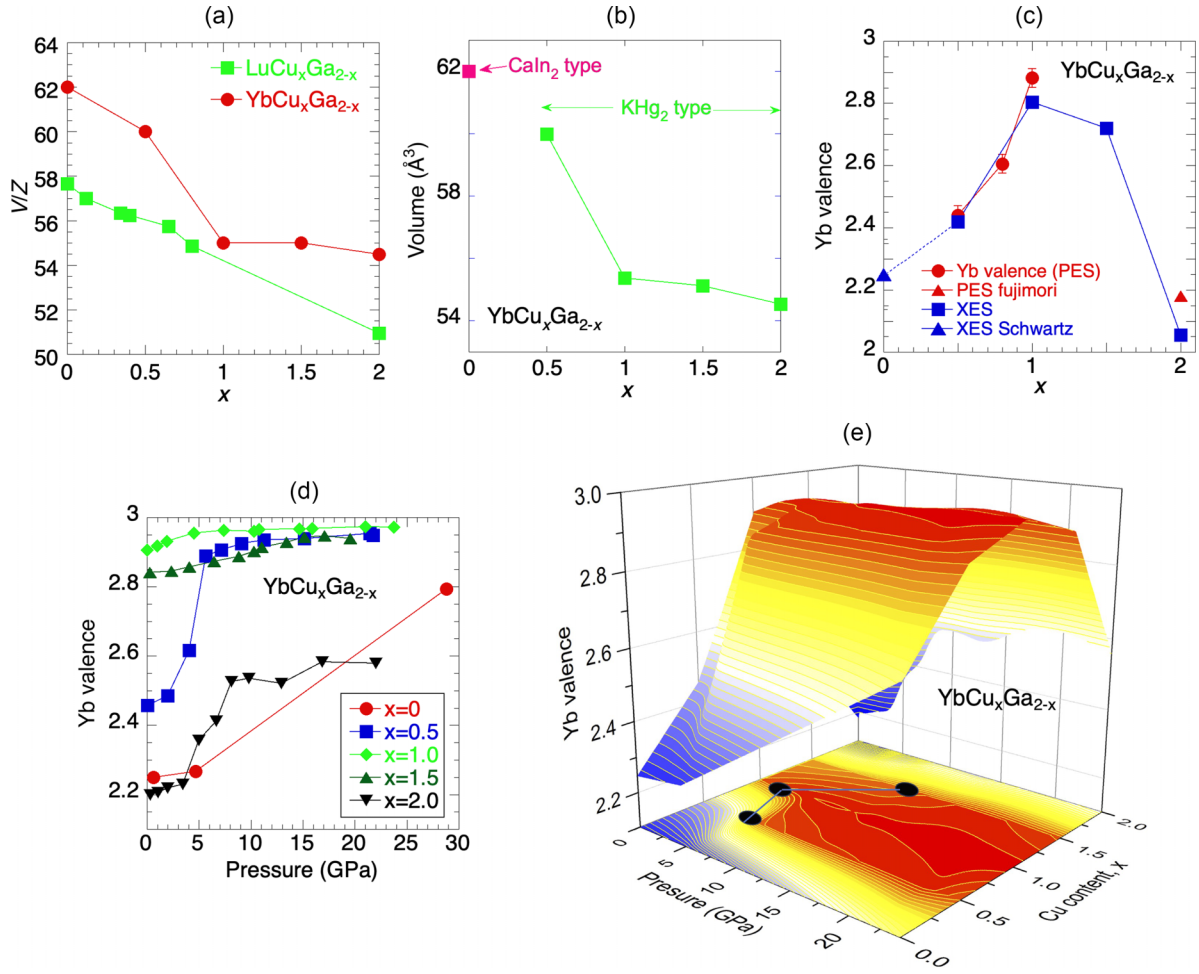

FIG. 6. (a) Lattice volume (V/Z) of LuCu$_x$Ga$_{2-x}$ as a function of x along with YbCu$_x$Ga$_{2-x}$, where Z is atomic number. (b) Chemical composition, Cu content x dependence of the volume of YbCu$_x$Ga$_{2-x}$. Here, we added the data of YbGa$_2$ although YbGa$_2$ have a different crystal structure of the CaIn$_2$ type. (c) Chemical composition dependence of the Yb valence obtained from the valence band spectra (closed circle) and the PFY-XAS spectra (closed square) as a function of x at ambient pressure except for the data at $x = 0$ (triangle) measured at 0.6 GPa [39]. The data at $x = 2.0$ (triangle and closed square) are taken from the Refs. [40,58]. The errors of the data of XES (closed square) are within the size of the symbol. (d) Pressure dependence of the Yb valence in YbCu$_x$Ga$_{2-x}$. (e) A summary of the chemical composition and pressure dependencies of the Yb valence. In (d) closed circles at the bottom correspond to the critical pressure where the large change in the Yb valences was observed.

where Cu atoms are covalently bonded to the O atoms, but similar to that of the metallic compound of YbInCu$_4$ [47]. Theoretical calculations for fcc and bcc Cu metal suggested that the first peak at 935 eV and the second peak at 939 eV corresponding to the transitions of 2p–3d and 2p–3s, respectively [45]. Figure 5(b) indicates that the XAS spectra at the Cu-L absorption edge do not show a significant difference among the above three samples. Figure 5(c) shows an expanded view of Fig. 5(b) around the absorption edge. Relative energy shift of the absorption edge to lower incident energy was observed as increasing the Cu content x.

Figure 5(d) shows valence band spectra measured at 4d–4f resonant energy of 182 eV and at 7–18 K [48,49]. The spectra consist of Yb^{2+} near the Fermi level and Yb^{3+} components with Cu 3d and Ga 3d peaks. The intensity of the Yb^{3+} component in YbCuGa is stronger than those in others, while the intensities of the Yb^{2+} component in YbCu$_{0.5}$Ga$_{1.5}$ and YbCu$_{0.8}$Ga$_{1.2}$ are stronger than that in YbCuGa When the intensity of the Yb^{2+} component is strong, the c–f hybridization is also usually strong in the Kondo system. Therefore, above results indicate stronger hybridization in YbCu$_{0.5}$Ga$_{1.5}$ and YbCu$_{0.8}$Ga$_{1.2}$ than that in YbCu$_{0.5}$Ga$_{1.5}$. This trend agrees with the results of the PFY-XAS as shown in the x dependence of the Yb valence in Fig. 6(b) below.

Bulk-sensitive high-resolution PES was also performed by using light of 8.4 eV from a Xe lamp at 7–8 K for YbCu$_{0.5}$Ga$_{1.5}$, YbCuGa, and YbCu$_{1.5}$Ga$_{0.5}$ as shown in Fig. 5(e). The peaks near the Fermi level and 1.5 eV are the components of 4$f_{7/2}$ and 4$f_{5/2}$, respectively. It is noted that in this incident photon energy range, the cross-section of the Yb 4f electrons is much smaller compared to that of Cu/Ga d and p electrons and, therefore, the valence band spectra mainly reflect the d and p states [50]. The density of states (DOS) at the Fermi level of YbCuGa is smaller than those of YbCu$_{0.5}$Ga$_{1.5}$ and YbCu$_{1.5}$Ga$_{0.5}$. The Yb valence of YbCuGa is closer to the Yb^{3+} state compared to the other samples, suggesting a weaker hybridization strength in YbCuGa than that in YbCu$_{0.5}$Ga$_{1.5}$ and YbCu$_{1.5}$Ga$_{0.5}$. In Yb metal and Yb

compounds, pressure induces the shift of the Yb^{2+} component toward the Fermi level, charge transfer occurs above the Fermi level, the intensity of Yb^{2+} component decreases, and a transition to the Yb^{3+} state occurs normally [51,52]. In YbCuGa the Yb valence is already near the Yb^{3+} state at ambient pressure and, therefore, it is reasonable that the transition pressure to the Yb^{3+} state for YbCuGa lower than those for $YbCu_{0.5}Ga_{1.5}$ and $YbCu_{1.5}Ga_{0.5}$ as shown in Fig. 4. Additionally, we measured the valence band spectra of $YbCu_{0.5}Ga_{1.5}$ around the Yb $4d$–$4f$ resonant energy. Details are shown in Fig. S3 within the SM [38].

IV. DISCUSSION

A. Chemical composition dependence

1. Comparison with the other similar Yb systems

We consider the chemical composition dependence of the electronic and crystal structures compared with the other similar Yb systems. It seems some parts of the characteristics of these materials cannot be explained by chemical pressure. Comparing this with $LuCu_xGa_{2-x}$ [53], this can be understood better. We plotted the normalized lattice volume (V/Z) of $LuCu_xGa_{2-x}$ as a function of x along with $YbCu_xGa_{2-x}$ as shown in Fig. 6(a), where V and Z are the lattice volume and the atomic number, respectively. $LuCu_xGa_{2-x}$ is considered to be consistently Lu^{3+} throughout. In general, V/Z changes linearly with respect to x (Vegards law). On the other hand, when considering the difference with $YbCu_xGa_{2-x}$, the difference is small near $x = 1$, so it is closer to Yb^{3+}. However, in $YbCu_xGa_{2-x}$ V/Z is large at $x = 0$, 0.5, and 1.0, so it is closer to Yb^{2+}. The effect of chemical pressure is apparent in the fact that the difference with $LuCu_xGa_{2-x}$ corresponds to the deviation of the Yb valence from 3+. However, we do not know why the shift becomes small near $x = 1$ and Yb^{3+} becomes stable, and it cannot be explained simply by chemical pressure. Instead, it is reasonable to assume that it is because the c–f hybridization strength changes because of the number of valence electrons, electronic state, band filling, etc. The present results suggested that the hybridization partner changes from Ga to Cu around $x = 1.0$–1.5; this expresses the same thing. Furthermore, in $YbCu_{5-x}Al_x$, as the lattice constant increases with x, the Yb^{2+} should increase from the viewpoint of chemical pressure, but in practice it approached Yb^{3+} [54]. This is the same as in the present case of $YbCu_{5-x}Ga_x$.

2. Defects or disorder

We compared the peak widths of the XRD pattern at three diffraction angles at ambient pressure when the chemical composition changed in $YbCu_xGa_{2-x}$ [38]. All results show the same tendency, with the peak width being almost the same at $x = 0.5$ and $x = 1.5$, slightly wider at $x = 1.5$, and much narrower at $x = 1.0$. The broadening of the peak width may correspond to lattice defects or disorder, and thus the samples of $x = 0.5$ and 1.5 may have more of these than the $x = 1.0$ sample. On the other hand, the result suggests that YbCuGa is the most stable compound with fewer defects or disorders.

Here, we also consider the effect of the defects and the disordered Griffiths phase although the Griffiths phase is a unique order close to the low-temperature magnetic order [55–57]. In comparison with the lattice volume of $LuCu_xGa_{2-x}$ in Fig. 6(a), only the region around $x = 1.0$ is unique, and not so much around $x = 0.5$ and 1.5. This possibly suggests that the problem is more with the number of valence electrons or band filling than with disorder in YbCuGa since YbCuGa may be the most stable compound with fewer defects as described above. On the other hand, for the samples with $x = 0.5$ and 1.5, the effects of the defects and disorders may not be ignored.

Additionally, in $YbCu_{5-x}Al_{x,Al}$ is also distributed randomly at the $3g$ site, but it transitions from the valence fluctuation state at $x = 0$ to QCP around $x = 1.5$ and antiferromagnetic order at $x = 2.0$, like a normal Doniach phase diagram, and further transitions in the opposite direction to the chemical pressure [54]. Therefore, even if there is a disorder in $YbCu_xGa_{2-x}$, the effect is more significantly influenced by changes in the electronic state.

3. Yb valence and crystal structure

The chemical composition dependence of the volume is shown in Fig. 6(b). The volume decreases rapidly between $x = 0.5$ and 1.0 and gradually between $x = 1.0$–2.0. The chemical composition dependence of the Yb valence estimated from the PFY-XAS and the valence band spectra at ambient pressure between $x = 0.5$–1.5 is shown in Fig. 6(c), with the data at $x = 0$ measured at 0.6 GPa [39], at $x = 2.0$ estimated from the valence band spectrum [58], and at $x = 2.0$ previously measured from the XAS spectrum [40]. The Yb valences derived from the valence band spectra show a trend to be larger than those from the PFY-XAS spectra. The Yb valence derived from the valence band spectra may remain the surface effect although we separate the surface component of the Yb^{2+} spectra [59]. The decrease of the Cu content induced the increase of the c–f hybridization at $x \leqslant 1$, resulting in the decrease of the Yb valence. As shown in Fig. 5(d), the spectra at the Cu-L absorption edge showed a shift to the lower incident energy with increasing the Cu content x between $x = 0.8$–1.5. A similar energy shift of the Cu absorption edge was observed in $YbInCu_4$ in the temperature-induced valence transition, where it has been considered that the charge transfer occurred between Yb and Cu [47,60]. The result of the energy shift of the Cu-L absorption edge supports the charge transfer with the increase of the Yb valence up to $x = 1.0$–1.5 in Fig. 6(c).

The atomic distances between Yb and M (M = Ga, Cu), the lattice constants, and the volume decreased with increasing x, the Cu content [38]. Here, the Yb valence increased with increasing the Cu content x at $x \leqslant 1$, suggesting the decrease of the c–f hybridization between Yb and Ga. It is reasonable to consider that the electron transfer may occur mainly between Yb $4f$ and Ga bands at $x \leqslant 1$ and the decrease of the Ga DOS may cause the decrease of the hybridization of Yb and Ga [38]. The Yb valence increases with decreasing the volume normally. Thus, both effects of the decreases of both the Ga DOS and the volume result in the increase of the Yb valence up to $x = 1.0$. Interestingly, in the region where Cu and Ga contents are comparable, the hybridization is the weakest and the Yb valence approaches 3+. On the other hand, the Yb-M

distances of $d2$ and $d3$ show an anomalous increase at $x = 1.5$ as shown in Fig. 3(e) (indicated by dotted circles). The atomic distances of $d1$ and $d4$ show a little change between $x = 1.5$–2.0 and also the volume decreases with x gradually at $x \geqslant 1.0$. These changes in the atomic distances at $x \geqslant 1.5$ seem to correlate to those in the Yb valences in Fig. 6(b).

Additionally, we note that in $YbAu_xGa_{2-x}$ a similar trend as in $YbCu_xGa_{2-x}$ was reported where the Yb valence took the maximum around $x \sim 1$ which correlated to the minimum of the volume [14]. However, in $YbCu_xGa_{2-x}$ the minimum of the volume does not correspond to the maximum of the Yb valence.

4. Atomic distances and ratio of the lattice constants

The atomic distances of $d1$ and $d4$ changed irregularly at $x \geqslant 1.5$ as described above with increasing the Cu content. We should, on the other hand, consider the fact that both the lattice constants and volume decreased as a whole with increasing x although the rate of decrease becomes smaller when $x > 1$. Therefore, the sudden large decrease of the Yb valence at $x = 2.0$ is anomalous. Another factor could be also considered as the origin of the rapid decrease of the Yb valence and increase of the hybridization at $x = 2.0$. At $x \geqslant 1.5$ the c–f hybridization between Yb $4f$ and Cu d may be enhanced largely because of both the effects of the increase of the Cu d DOS and the decrease of the Yb–Cu atomic distances. Our preliminary DFT calculation results (not considering hybridization) support this scenario that increasing x makes Cu d DOS much stronger in particular at $x \geqslant 1.5$ [38]. Further detailed calculations taking into account the hybridization remain challenging in the future. The present results indicate that in $YbCu_xGa_{2-x}$ the hybridization partner of Yb switched from Ga to Cu with increasing the Cu content around $x = 1.0$–1.5, where the hybridization became minimum.

We add that the x dependence of the ratios of the lattice constants, a/b and a/c, correlates to that of the Yb valence, while the ratio of b/c inversely correlates to that as shown in Figs. 2(d)–2(f). It seems to suggest that the lattice shrink in the bc plane, i.e., the change in the distance d, is important for the change in the Yb valence although the exact physical meaning is unclear.

B. Pressure dependence

1. Yb valence transition

Figure 6(c) shows the chemical composition and pressure dependencies of the Yb valence in $YbCu_xGa_{2-x}$. The Yb valence of $YbGa_2$ is included as a reference although it has a different crystal structure of $CaIn_2$ at ambient pressure [39]. In $YbGa_2$ Schwartz *et al.* [39] measured the pressure dependence of the XAS spectra at the Yb-L_3 absorption edge at three pressure points of 0.6, 4.7, and 28.8 GPa, but the values of the Yb valence were not estimated. Here, we analyzed their data and added the estimated values of the Yb valences in Figs. 6(c) and 6(d) [38].

It is known that in most Yb compounds the magnetic order occurs at relatively high Yb valence values of more than 2.7 [61]. YbCuGa showed already a relatively high Yb valence of 2.91 at ambient pressure. However, YbCuGa was considered to be in the Fermi liquid ground state at ambient pressure [8,9], and the Yb valence increased to be approximately 2.96 around 5 GPa with pressure. In $YbCu_{0.5}Ga_{1.5}$ and $YbCu_{1.5}Ga_{0.5}$ the Yb valence increased similarly from 2.4 and 2.84 at ambient pressure to approximately 2.9 around 10 GPa and 2.94 around 15 GPa, respectively.

In Yb compounds, the Kondo temperature decreases with pressure and the Yb^{3+} state is favored. Some Yb compounds showed the pressure-induced change from the Fermi liquid ground state to the magnetic order state via QCP [18,32,62–64]. These systems show little change in the Yb valence at the pressures above QCP. QCP is defined to appear at low temperatures of nearly 0 K. The Yb valence normally decreases with decreasing temperature and thus, the valence fluctuation may be enhanced at low temperatures. However, a relative change in the Yb valence in the pressure dependence is considered to be similar to that at room temperature [63]. Furthermore, the temperature dependence of Yb valence at ambient pressure showed only a relatively small change of 0.02 to 0.04 [65]. Therefore, YbCuGa may have QCP around $P_v = 2.5$ GPa. In $YbCu_{0.5}Ga_{1.5}$ temperature dependence of the electrical resistivity under pressure will show anomaly with the hysteresis and the divergent behavior of the A coefficient at P_v as observed in the Eu compounds [66,67] if this system is in the Fermi liquid state at low temperatures. Such a study of the transport properties under pressure is expected.

$YbGa_2$ shows a large pressure-induced change in the Yb valence similar to the case of $YbCu_{0.5}Ga_{1.5}$ and therefore, we could expect a first-order valence transition also in $YbGa_2$ between 5 and 30 GPa. The first-order valence transition in $YbGa_2$ has not been confirmed yet because of too few data points in the measurements by Schwartz *et al.* [39].

In Fig. 6(e) we show a summary of the chemical and pressure dependence of the Yb valence. At both the Cu content end sides of $x = 0$ and 2.0, the Yb valences are on the order of 2.2, divalent side at ambient pressure, while they are 2.8–2.9 around $x = 1.0$–1.5 around the region where the Cu and Ga contents are comparable. The result indicates that the unoccupied states above the Fermi level are little around $x = 1.0$–1.5 with small DOS hybridized weakly, while there are many unoccupied states at $x = 0$ and 2.0 with large DOS of Ga or Cu hybridized strongly [51]. In any case, pressure-induced the increase of the charge transfer from Yb to the unoccupied states of Ga or Cu, resulting in the increase of the Yb valence.

2. Comparison with other Yb compounds

In $Yb_xFe_4Sb_{12}$, there was a mechanism whereby the change in the valence occurred because of the charge transfer to Yb vacancy sites [68]. In $YbCu_{0.5}Ga_{1.5}$ the change in the valence under pressure occurred suddenly. Therefore, a similar charge transfer caused by the defects in $YbCu_{0.5}Ga_{1.5}$ could be considered. However, the EPMA analyses showed large errors in the Yb composition ratio as described above. There could be defects at the Yb site that play an important role in the charge transfer, but this cannot be said with certainty from the present results. At present, it may be more reasonable to think that the change in the valence is linked

to continuously changing factors such as the bandwidth and density of states, that is, reflecting the change in the c–f hybridization. As another example of a continuous change in valence because of pressure even in the presence of disorder, we would like to cite a paper on the YbGaSi system [69].

V. CONCLUSIONS

We establish phase diagrams for the change in the crystal structure and the Yb valence in $YbCu_xGa_{2-x}$ as a function of chemical composition and pressure.

Pressure-induced changes in the electronic structure of $YbCu_xGa_{2-x}$ were studied by high-resolution XAS with a partial fluorescence mode at the Yb-L_3 absorption edge. In $YbCu_{0.5}Ga_{1.5}$ the first-order transition of the Yb valence was found around 5 GPa, where the Yb valence increased largely from 2.6 to 2.9. The Yb valence of YbCuGa and $YbCu_{1.5}Ga_{01.5}$ successively increased up to 5 and 15 GPa, respectively, and it did not show a significant change above those pressures.

XRD study showed the structural phase transition in $YbCu_{0.5}Ga_{1.5}$ at the same pressure range of the valence transition, indicating the valence transition induced by the structural phase transition. We clarified the crystal structure of KHg_2-type at ambient pressure for $YbCu_{0.5}Ga_{1.5}$. The space group of *Pmmb* with orthorhombic symmetry was suggested as a crystal structure at high pressures after the phase transition in $YbCu_{0.5}Ga_{1.5}$. $YbCu_{1.5}Ga_{0.5}$ and YbCuGa did not show the structural transition up to 15 GPa and 13 GPa, respectively.

The XAS spectra at the Cu-L absorption edge showed a shift of the edge energy to the lower incident energy with increasing x. At $x \leqslant 1$ the c–f hybridization occurred mainly between Yb and Ga, while the c–f hybridization between Yb and Cu may be enhanced at $x \geqslant 1.5$ because of both effects of the increase of the Cu DOS and decrease of the atomic distances between Yb and Cu. In $YbCu_xGa_{2-x}$ the main hybridization partner of Yb $4f$ electrons switched from Ga to Cu with increasing the Cu content around $x = 1$–1.5, where the c–f hybridization became minimum.

ACKNOWLEDGMENTS

The experiments were performed at Taiwan beamlines BL12XU and BL12B1 at SPring-8 under Proposals No. 2014B4257, No. 2015A4129, No. 2015A4258, No. 2015B4258, and No. 2015B4133 (corresponding Proposals No. 2014-3-003 and No. 2015-2-033 of NSRRC) and also beamlines BL-7, BL-9 (Xe lamp), and BL-14 at HiSOR under Proposals No. 15-A-3, No. 16AG003, and No. 16AG004. We thank the N-BARD, Hiroshima University, for supplying the liquid helium. This work is supported by Grants in Aid for Scientific Research from the Japan Society for the Promotion of Science (Kiban C 15K05194, Kiban C 15K05190, Kiban Houga 18K18743, and Kiban Houga 24K21692).

[1] J. M. Lawrence, P. S. Riseborough, and R. D. Parks, Valence fluctuation phenomena, Rep. Prog. Phys. **44**, 1 (1981).

[2] S. Doniach, The Kondo lattice and weak antiferromagnetism, Physica B+C **91**, 231 (1977).

[3] E. Bauer, Anomalous properties of Ce-Cu- and Yb-Cu-based compounds, Adv. Phys. **40**, 417 (1991).

[4] P. Coleman, C. Pépin, Q. Si, and R. Ramazashvili, How do Fermi liquids get heavy and die? J. Phys.: Condens. Matter **13**, R723 (2001).

[5] H. v. Löhneysen, A. Rosch, M. Vojta, and P. Wölfle, Fermi-liquid instabilities at magnetic quantum phase transitions, Rev. Mod. Phys. **79**, 1015 (2007).

[6] P. Coleman, Heavy fermions and the Kondo lattice: A 21st century perspective, in *Many-Body Physics: From Kondo to Hubbard Modeling and Simulation*, edited by E. Pavarini, E. Koch, and P. Coleman (Forschungszentrum Jülich GmbH Institute for Advanced Simulation, 2015), Vol. 5.

[7] S. K. Malik, D. T. Adroja, B. D. Padalia, and R. Vijayaraghavan, Studies on the valence state of Yb in YbTGa (T = Cu, Pd and Pt) compounds through magnetic susceptibility measurements, Jpn. J. Appl. Phys. **26**, 553 (1987).

[8] D. T. Adroja, S. K. Malik, B. D. Padalia, S. N. Bhatia, R. Walia, and R. Vijayaraghavan, Valence-fluctuation behavior of Yb ions in YbCuGa, Phys. Rev. B **42**, 2700 (1990).

[9] D. T. Adroja, B. D. Rainford, L. E. Miller, and S. K. Malik, Neutron scattering and transport studies of YbTGa compounds (T = Cu, Pd and Pt), Phys. B: Condens. Matter **230-232**, 282 (1997).

[10] D. Rossi and R. Ferro, Ternary intermetallic RAgGa, RAuGa alloys (R = light rare earth and Yb), J. Alloys Compd. **317-318**, 521 (2001).

[11] U. Burkhardt, R. Niewa, M. Schmidt, R. Gumeniuk, L. Vasylechko, and Y. Grin, Pressure dependence of Yb valence state of some ternary ytterbium–transition metal–gallides, HASYLAB Annual Report 2003, https://hasyweb.desy.de/science/annual_reports/2003_report/.

[12] M. K. Reimann, H. Kohlmann, S. F. Matar, and R. Pöttgen, Ternary magnesium gallides–synthesis, crystal chemistry and properties of CaMgGa, SrMgGa, BaMgGa and YbMgGa, Z. Anorg. Allg. Chem. **649**, e202200361 (2023).

[13] U. Schwarz, M. Schmidt, R. Gumeniuk, W. Schnelle, M. Hanfland, K. Klementiev, and Yu. Grin, Chemical bonding and pressure-induced change of the electron configuration of ytterbium in β-$YbAgGa_2$, Z. Anorg. Allg. Chem. **630**, 122 (2004).

[14] R. Gumeniuk, E. Bischoff, U. Burkhardt, Yu. Prots, W. Schnelle, L. Vasylechko, M. Schmidt, Yu. Kuzma, and Yu. Grin, Orderdisorder transition and valence state of ytterbiumin $YbAu_xGa_{2-x}$ ($0.26 < x < 1.31$), J. Solid State Chem. **182**, 3374 (2009).

[15] E. Bauer, Le Tuan, R. Hauser, E. Gratz, T. Holubar, G. Hilscher, H. Michor, W. Perthold, C. Godart, E. Alleno, and K. Hiebl, Evolution of a magnetic state in $YbCu_{5-x}Ga_x$, Phys. Rev. B **52**, 4327 (1995).

[16] U. Subbarao and S. C. Peter, Crystal growth and properties of $YbCuGa_3$: First monoclinic system in the $RETX_3$ family, Cryst. Growth Des. **13**, 953 (2013).

[17] Z. E. Brubaker, R. L. Stillwell, P. Chow, Y. Xiao, C. Kenney-Benson, R. Ferry, D. Popov, S. B. Donald, P. Söderlind, D. J. Campbell, J. Paglione, K. Huang, R. E. Baumbach, R. J. Zieve, and J. R. Jeffries, Pressure-dependent intermediate valence behavior in $YbNiGa_4$ and $YbNiIn_4$, Phys. Rev. B **98**, 214115 (2018).

[18] K. Matsubayashi, T. Hirayama, T. Yamashita, S. Ohara, N. Kawamura, M. Mizumaki, N. Ishimatsu, S. Watanabe, K. Kitagawa, and Y. Uwatoko, Pressure-induced valence crossover and novel metamagnetic behavior near the antiferromagnetic quantum phase transition of $YbNi_3Ga_9$, Phys. Rev. Lett. **114**, 086401 (2015).

[19] K. Umeo, T. Otaki, Y. Arai, S. Ohara, and T. Takabatake, Pressure-induced quantum critical behavior and magnetic order in $YbNi_3Ga_9$ with a chiral crystal structure: ac calorimetric measurements up to 12 GPa, Phys. Rev. B **98**, 024420 (2018).

[20] H. Okamura, A. Takigawa, T. Yamasaki, E. D. Bauer, S. Ohara, Y. Ikemoto, and T. Moriwaki, Contrasting pressure evolution of f-electron hybridized states in $CeRhIn_5$ and $YbNi_3Ga_9$: An optical conductivity study, Phys. Rev. B **100**, 195112 (2019).

[21] Y. Utsumi, D. Mondal, J. Fujii, I. Vobornik, S. Nakamura, D. Matković-Čalogović, and S. Ohara, Electronic structure of $Yb(Ni_{1-x}Co_x)_3Ga_9$ studied by angle-resolved photoelectron spectroscopy, J. Phys. Soc. Jpn. **89**, 044711 (2020).

[22] D. Mumbaraddi, V. Mishra, S. Lidin, and A. Mar, Minority report: Structure and bonding of $YbNi_3Ga_9$ and $YbCu_3Ga_8$ obtained in gallium flux, J. Solid State Chem. **311**, 123157 (2022).

[23] M. Schlüter and W. Jeitschko, Ternary lanthanoid ruthenium gallides with a high gallium content: $Ln_2Ru_3Ga_{10}$ (Ln = Yb, Lu) with a new structure type and $LnRu_2Ga_8$ (Ln = La–Nd) with $CaCo_2Al_8$-type structure, Inorg. Chem. **40**, 6362 (2001).

[24] A. Rousuli, S. Nakamura, H. Sato, T. Ueda, Y. Matsumoto, S. Ohara, E. F. Schwier, T. Nagasaki, K. Mimura, H. Anzai, K. Ichiki, S. Ueda, K. Shimada, H. Namatame, and M. Taniguchi, Photoemission study of the electronic structure of the Kondo lattices $Yb_2Pt_6X_{15}$ (X = Al, Ga), Phys. Rev. B **96**, 045117 (2017).

[25] K. Hämäläinen, D. P. Siddons, J. B. Hastings, and L. E. Berman, Elimination of the inner-shell lifetime broadening in x-ray-absorption spectroscopy, Phys. Rev. Lett. **67**, 2850 (1991).

[26] K. Hämäläinen, C. C. Kao, J. B. Hasting, D. P. Siddons, L. E. Berman, V. Stojanoff, and S. P. Cramer, Spin-dependent x-ray absorption of MnO and MnF_2, Phys. Rev. B **46**, 14274 (1992).

[27] J.-P. Rueff and A. Shukla, Inelastic x-ray scattering by electronic excitations under high pressure, Rev. Mod. Phys. **82**, 847 (2010).

[28] A. P. Hammersley, S. O. Svensson, M. Hanfland, A. N. Fitch, and D. Hausermann, Two-dimensional detector software: From real detector to idealised image or two-theta scan, High Press. Res. **14**, 235 (1996).

[29] Jana2006 program to analyze the crystal structures, http://jana.fzu.cz/.

[30] V. Petříček, M. Dusek, and L. Palatinus, Crystallographic computing system JANA2006: General features, Z. Kristallogr. **229**, 345 (2014).

[31] H. Yamaoka, Pressure dependence of the electronic structure of $4f$ and $3d$ electron systems studied by x-ray emission spectroscopy, High Press. Res. **36**, 262 (2016).

[32] H. Yamaoka, I. Jarrige, N. Tsujii, J.-F. Lin, N. Hiraoka, H. Ishii, and K.-D. Tsuei, Temperature and pressure-induced valence transitions in $YbNi_2Ge_2$ and $YbPd_2Si_2$, Phys. Rev. B **82**, 035111 (2010).

[33] H.-K. Mao and P. M. Bell, High-pressure physics: The 1-megabar mark on the ruby R_1 static pressure scale, Science **191**, 851 (1976).

[34] K. Syassen, Ruby under pressure, High Press. Res. **28**, 75 (2008).

[35] H. Yamaoka, Y. Zekko, I. Jarrige, J.-F. Lin, N. Hiraoka, H. Ishii, K.-D. Tsuei, and J. Mizuki, Ruby pressure scale in a low-temperature diamond anvil cell, J. Appl. Phys. **112**, 124503 (2012).

[36] M. Sawada, K. Yaji, M. Nagira, A. Kimura, H. Namatame, and M. Taniguchi, Design concept and performance of the soft x-ray beamline HiSOR-BL14, AIP Conf. Proc. **879**, 551 (2007).

[37] Peasons' Crystal Data Base https://www.crystalimpact.com/pcd/. Original data was found in a reference V. Y. Markiv, N. N. Belyavina, and T. I. Zhunkovskaya, The x-ray structure investigation of the Y-Cu-Ga system alloys and RECu2-REGa2 sections, Dopov. Akad. Nauk Ukr. RSR, Ser. A 2, 80 (1982).

[38] See Supplemental Material at http://link.aps.org/supplemental/10.1103/PhysRevB.110.205129 for (i) calculated results after the phase transition using several structure models and refined Yb site occupancy of $YbCu_{0.5}Ga_{1.5}$, (ii) examples of the fit to the XRD pattern, results of structure refinements and final parameters used for the analyses, (iii) XAS spectra of $YbGa_2$ [39] and the estimated Yb valence, (iv) an explanation of the modified logistic curve, (v) additional results of the resonant photoelectron spectroscopy for $YbCu_{0.5}Ga_{1.5}$, and (v) partial DOS of the band calculations, which includes Refs. [37,39,40,48,49,51,58,70–72].

[39] U. Schwarz, R. Giedigkeit, R. Niewa, M. Schmidt, W. Schnelle, R. Cardoso, M. Hanfland, Z. Hu, K. Klementiev, and Yu. Grin, Pressure-induced oxidation state change of ytterbium in $YbGa_2$, Z. Anorg. Allg. Chem. **627**, 2249 (2001).

[40] H. Yamaoka, A. Ohmura, N. Tsujii, H. Ishii, N. Hiraoka, H. Sato, and M. Sawada, Pressure-induced large valence transitions in Yb-Cu binary intermetallic systems, Phys. Rev. B **109**, 155147 (2024).

[41] F. D. Murnaghan, The compressibility of media under extreme pressures, Proc. Natl. Acad. Sci. USA **30**, 244 (1944).

[42] Inorganic Crystal Structure Database (ICSD, https://icsd.fiz-karlsruhe.de) with the PDF number 01-071-7915 for $YbCu_2$ and 01-082-6291 for $YbCu_{0.8}Ga_{1.2}$.

[43] H. Yamaoka, N. Tsujii, K. Yamamoto, A. M. Vlaicu, H. Oohashi, H. Yoshikawa, T. Tochio, Y. Ito, A. Chainani, and S. Shin, Bulk sensitive spectroscopy in the valence transition of $YbInCu_4$-based compounds, Phys. Rev. B **78**, 045127 (2008).

[44] M. Finazzi, G. Ghiringhelli, O. Tjernberg, Ph. Ohresser, and N. B. Brookes, Radiationless Raman versus Auger behavior at the Cu L_3 resonance of CuO and Cu_2O, Phys. Rev. B **61**, 4629 (2000).

[45] H. Ebert, J. Stöhr, S. S. P. Parkin, M. Samant, and A. Nilsson, L-edge x-ray absorption in fcc and bcc Cu metal: Comparison of experimental and first-principles theoretical results, Phys. Rev. B **53**, 16067 (1996).

[46] P. Jiang, D. Prendergast, F. Borondics, S. Porsgaard, L. Giovanetti, E. Pach, J. Newberg, H. Bluhm, F. Besenbacher, and

M. Salmeron, Experimental and theoretical investigation of the electronic structure of Cu_2O and CuO thin films on Cu(110) using x-ray photoelectron and absorption spectroscopy, J. Chem. Phys. **138**, 024704 (2013).

[47] Y. Utsumi, H. Sato, H. Kurihara, H. Maso, K. Hiraoka, K. Kojima, K. Tobimatsu, T. Ohkochi, S. Fujimori, Y. Takeda, Y. Saitoh, K. Mimura, S. Ueda, Y. Yamashita, H. Yoshikawa, K. Kobayashi, T. Oguchi, K. Shimada, H. Namatame, and M. Taniguchi, Conduction-band electronic states of $YbInCu_4$ studied by photoemission and soft x-ray absorption spectroscopies, Phys. Rev. B **84**, 115143 (2011).

[48] H. Yamaoka, P. Thunström, N. Tsujii, I. Jarrige, K. Shimada, M. Arita, H. Iwasawa, H. Hayashi, J. Jiang, H. Namatame, M. Taniguchi, N. Hiraoka, H. Ishii, K.-D. Tsuei, M. Giovannini, and E. Bauer, Electronic structure and the valence state of Yb_2Pd_2Sn and $YbPd_2Sn$ studied by photoelectron and resonant x-ray emission spectroscopies, Phys. Rev. B **86**, 085137 (2012).

[49] H. Yamaoka, P. Thunström, N. Tsujii, K. Katoh, Y. Yamamoto, E. F. Schwier, K. Shimada, H. Iwasawa, M. Arita, I. Jarrige *et al.*, Electronic structure of ferromagnetic heavy fermion, YbPdSi, YbPdGe, and YbPtGe studied by photoelectron spectroscopy, x-ray emission spectroscopy, and DFT + DMFT calculations, J. Phys.: Condens. Matter **29**, 475502 (2017).

[50] J. J. Yeh and I. Lindau, Atomic subshell photoionization cross sections and asymmetry parameters: $1 \leqslant Z \leqslant 103$, At. Data Nucl. Data Tables **32**, 1 (1985).

[51] I. Jarrige, H. Yamaoka, J.-P. Rueff, J.-F. Lin, M. Taguchi, N. Hiraoka, H. Ishii, K.-D. Tsuei, K. Imura, T. Matsumura, A. Ochiai, H. S. Suzuki, and A. Kotani, Unified understanding of the valence transition in the rare-earth monochalcogenides under pressure, Phys. Rev. B **87**, 115107 (2013).

[52] E. R. Ylvisaker, J. Kuneš, A. K. McMahan, and W. E. Pickett, Charge fluctuations and the valence transition in Yb under pressure, Phys. Rev. Lett. **102**, 246401 (2009).

[53] V. Ya. Markiv, I. P. Shevchenko, and N. N. Bekyavina, Phase-equilibria and crystalline-structure of a compound in the Lu-Cu-Ga system, Russian Metallurgy (Metally) **2**, 201 (1989).

[54] H. Yamaoka, I. Jarrige, N. Tsujii, N. Hiraoka, H. Ishii, and K.-D. Tsuei, Temperature dependence of the Yb valence in $YbCu_5$ and $YbCu_{5-x}Al_x$ Kondo compounds studied by x-ray spectroscopy, Phys. Rev. B **80**, 035120 (2009).

[55] R. B. Griffiths, Nonanalytic behavior above the critical point in a random Ising ferromagnet, Phys. Rev. Lett. **23**, 17 (1969).

[56] R. Tripathi, D. T. Adroja, Y. Muro, S. Sharma, P. K. Biswas, T. Namiki, T. Kuwai, T. Hiroto, A. M. Strydom, A. Sundaresan, and S. Langridge, Quantum Griffiths singularity in the stoichiometric heavy-fermion system $CeRh_4Al_{15}$, Phys. Rev. B **108**, 144427 (2023).

[57] Y. Zhao, M. Tripathi, K. Čerevičs, A. Avsar, H. G. Ji, J. F. G. Marin, C.-Y. Cheon, Z. Wang, O. V. Yazyev, and A. Kis, Electrical spectroscopy of defect states and their hybridization in monolayer MoS_2, Nat. Commun. **14**, 44 (2023).

[58] A. Fujimori, T. Shimizu, and H. Yasuoka, Photoemission study of valence fluctuation in $YbCu_2$, Phys. Rev. B **35**, 8945 (1987).

[59] L. Moreschini, C. Dallera, J. J. Joyce, J. L. Sarrao, E. D. Bauer, V. Fritsch, S. Bobev, E. Carpene, S. Huotari, G. Vankó, G. Monaco, P. Lacovig, G. Panaccione, A. Fondacaro, G. Paolicelli, P. Torelli, and M. Grioni, Comparison of bulk-sensitive spectroscopic probes of Yb valence in Kondo systems, Phys. Rev. B **75**, 035113 (2007).

[60] H. Yamaoka, A. Ohmura, Y. Furue, N. Tsujii, H. Ishii, and N. Hiraoka, Direct observation of pressure-induced Yb valence transition in $YbInCu_4$, J. Phys. Soc. Jpn. **90**, 124801 (2021).

[61] B. T. Chiogo, N. P. Martin, L. V. B. Diop, B. Malaman, D. Malterre, F. Baudelet, L. Nataf, and T. Mazet, Temperature and pressure dependence of the Yb valence state in $YbMn_{\sim 0.17}Si_{\sim 1.89}$, J. Appl. Phys. **132**, 205902 (2022).

[62] H. Yamaoka, N. Tsujii, Y. Utsumi, H. Sato, I. Jarrige, Y. Yamamoto, J.-F. Lin, N. Hiraoka, H. Ishii, K.-D. Tsuei, and J. Mizuki, Valence transitions in the heavy-fermion compound YbCuAl as a function of temperature and pressure, Phys. Rev. B **87**, 205120 (2013).

[63] H. Sato, H. Yamaoka, Y. Utsumi, H. Nagata, M. A. Avila, R. A. Ribeiro, K. Umeo, T. Takabatake, Y. Zekko, J. Mizuki, J.-F. Lin, N. Hiraoka, H. Ishii, K.-D. Tsuei, H. Namatame, and M. Taniguchi, Pressure-induced valence change of $YbNiGe_3$ investigated by resonant x-ray emission spectroscopy at the Yb L_3 edge, Phys. Rev. B **89**, 045112 (2014).

[64] W. B. Jiang, L. Yang, C. Y. Guo, Z. Hu, J. M. Lee, M. Smidman, Y. F. Wang, T. Shang, Z. W. Cheng, F. Gao *et al.*, Crossover from a heavy fermion to intermediate valence state in noncentrosymmetric $Yb_2Ni_{12}(P, As)_7$, Sci. Rep. **5**, 17608 (2015).

[65] N. Tsujii *et al.*. (unpublished).

[66] F. Honda, K. Okauchi, A. Nakamura, D. Aoki, H. Akamine, Y. Ashitomi, M. Hedo, T. Nakama, and Y. Ōnuki, Pressure evolution of characteristic electronic states in $EuRh_2Si_2$ and $EuNi_2Ge_2$, J. Phys.: Conf. Ser. **807**, 022004 (2017).

[67] Y. Ashitomi, M. Kakihana, F. Honda, A. Nakamura, D. Aoki, Y. Uwatoko, M. Nakashima, Y. Amako, T. Takeuchi, T. Kida *et al.*, Magnetic properties and effect of pressure on the electronic state of $EuCo_2Ge_2$, Phys. B: Condens. Matter **536**, 192 (2018).

[68] I. Yamaoka, I. Jarrige, N. Tsujii, J.- Fu Lin, T. Ikeno, Y. Isikawa, K. Nishimura, R. Higashinaka, H. Sato, N. Hiraoka, H. Ishii, and K.-D. Tsuei, Strong coupling between $4f$ valence instability and $3d$ ferromagnetism in $Yb_xFe_4Sb_{12}$ studied by resonant x-ray emission spectroscopy, Phys. Rev. Lett. **107**, 177203 (2011).

[69] H. Yamaoka, I. Jarrige, N. Tsujii, M. Imai, J.-Fu Lin, M. Matsunami, R. Eguchi, M. Arita, K. Shimada, H. Namatame, M. Taniguchi, M. Taguchi, Y. Senba, H. Ohashi, N. Hiraoka, H. Ishii, and K.-D. Tsuei, Electronic structure of $YbGa_{1.15}Si_{0.85}$ and $YbGa_xGe_{2-x}$ probed by resonant x-ray emission and photoelectron spectroscopies, Phys. Rev. B **83**, 104525 (2011).

[70] R.-D. Hoffmann and R. Pöttgen, AlB_2-related intermetallic compounds—a comprehensive view based on group-subgroup relations, Z. Kristallogr. **216**, 127 (2001).

[71] WIEN2k: An APW + lo program for calculating the properties of solids, http://susi.theochem.tuwien.ac.at/.

[72] P. Blaha, K. Schwarz, F. Tran, R. Laskowski, G. K. H. Madsen, and L. D. Marks, WIEN2k: An APW + lo program for calculating the properties of solids, J. Chem. Phys. **152**, 074101 (2020).